Study of alpha particle properties across rarefaction regions

Tereza Ďurovcová[A], Jana Šafránková, and Zdeněk Němeček

Faculty of Mathematics and Physics, Charles University, Prague, Czech Republic

[A] *tereza.durovcova@mff.cuni.cz*

1. Abstract

Two large-scale interaction regions between the fast solar wind emanating from coronal holes and the slow solar wind coming from streamer belt are usually distinguished. When the fast stream pushes up against the slow solar wind ahead of it, a compressed interaction region that co-rotates with the Sun (CIR) is created. Ďurovcová et al. (2019) showed that the relative abundance of alpha particles, which usually serve as one of solar wind source identifiers can change within these regions. By symmetry, when the fast stream outruns the slow stream, a corotating rarefaction region (CRR) is formed. CRRs are characterized by a monotonic decrease of the solar wind speed, and they are associated with the regions of small longitudinal extent on the Sun. In our study, we use near-Earth measurements, and focus on the behavior of alpha particles in the CRRs because we found that the large variations of the relative helium abundance (AHe) can also be observed there. Unlike in the CIRs, these variations are usually not connected with the solar wind speed and alpha-proton relative drift changes. We thus apply a superposed-epoch analysis of identified CRRs with a motivation to determine the global profile of alpha particle parameters through these regions. Next, we concentrate on the cases with largest AHe variations and investigate whether they can be associated with the changes of the solar wind source region or whether there is a relation between the AHe variations and the non-thermal features in the proton velocity distribution functions like the temperature anisotropy and/or presence of the proton beam.

2. Corotating rarefaction regions

As noted, properties of alpha particles usually serve as one of the solar wind source identifiers. In the typical slow solar wind, the relative alpha abundance is low (about one percent) and highly variable. Alpha-proton relative drift is close to zero and protons move a bit faster than alphas. Temperatures of both ion species are balanced. On the other hand, in the high speed streams, all these features are significantly higher. Across CRRs, the profile of alpha particles should correspond to transition between the two shearing streams.

Borovsky and Denton (2016) studied a structure of high-speed stream trailing edges at 1 AU and summarized their finding by a sketch shown in Figure 1 (left). The initial velocity drop corresponds to the start of the CRR rarefaction, but there is evidence indicating that the rarefaction might start sooner. Identifying stream interface in the CRR is not straightforward. Stream interface signatures (such as composition change, drop in the specific entropy, velocity-bend, etc.) are temporally separated. In Figure 1 (top), 1D numerical simulations performed by Borovsky and Denton (2016) show that the velocity-bend is the collision point of the pressure driven expansions of the slow wind originating at streamer belt and the fast wind expanding from coronal hole. Thus, the velocity-bend is taken as the location of the CRR stream interface.

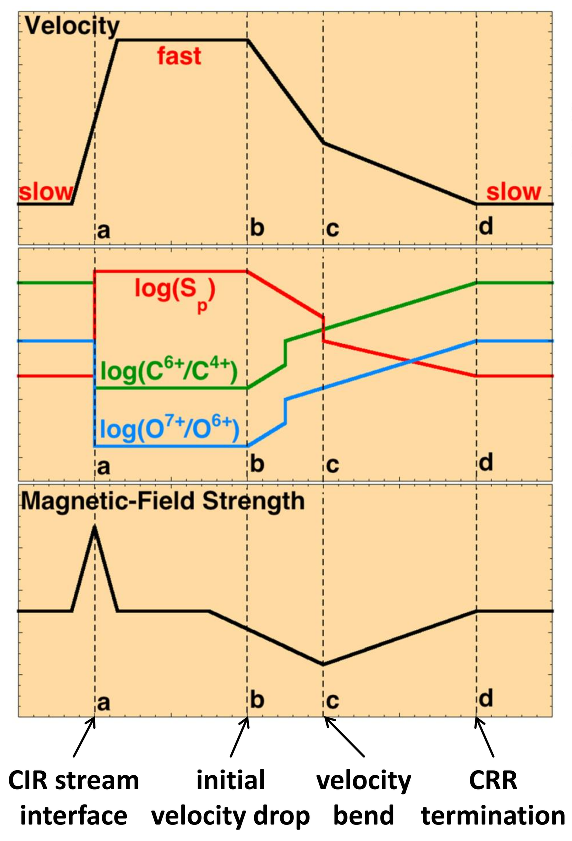

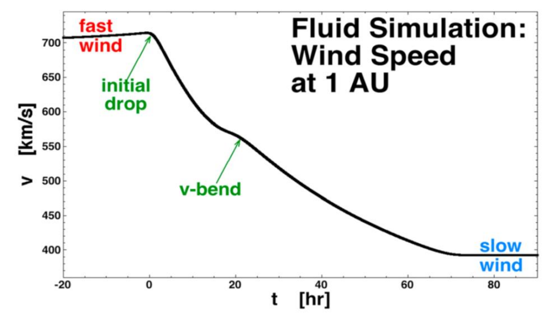

Figure 1: (left) The sketch (adopted from Borovsky and Denton, 2016) illustrates the chronology of major signatures in the high-speed stream and its surrounding at 1 AU. From top to bottom: proton bulk speed, specific entropy and heavy-ion charge state density ratios, and magnitude of the magnetic field. The four vertical dashed lines are the occurrence times of the CIR stream interface, the initial velocity drop, the velocity-bend and the termination of a trailing edge. (top) The velocity profile across CRR obtained from the 1D numerical simulations (adopted from Borovsky and Denton, 2016).

3. Case selection

We use the collection of 54 CRRs observed at 1 AU in the years 1998–2008 and collected by Borovsky and Denton (2016).

Selection criteria:

1. The trailing edge must be preceded by a robust high-speed stream with the duration of a day or more;
2. The trailing edge must have quasi-monotonic velocity profile without discontinuities or multiple velocity bend points;
3. A trailing edge is rejected if it contains clear signatures of ejecta (such as depressed proton temperature, long duration out-of-ecliptic magnetic field vectors, or bidirectional electron strahl);
4. The velocity within the trailing edge should eventually reach low speeds (≈400 km/s or less).

To these cases, we added the region of a quiet fast solar wind which preceded the CRR. The observation time of CRR regions varies considerably in different cases. Therefore, we divided the cases into 4 sub-intervals (fast stream – initial velocity drop, initial velocity drop – velocity bend, velocity bend – CRR termination, CRR termination – 6 hours after CRR termination).

In the whole analysis, we use the data measured by the SWE instrument onboard the Wind spacecraft.

4. Case study

Figure 2 shows two examples of the studied CRRs. Alpha properties typical for the slow solar wind streams appear at different times within the CRRs. First, the alpha-proton relative drift (5th panel) close to zero is observed near the velocity-bend. Then, towards the CRR termination, the alpha thermal speed (7th panel) starts to be lower than the proton thermal speed. The large changes in the relative alpha abundance are observed throughout the CRR (3rd panel). Near the CRR termination, alphas finally reach the abundance similar to that typically observed in the slow streams.

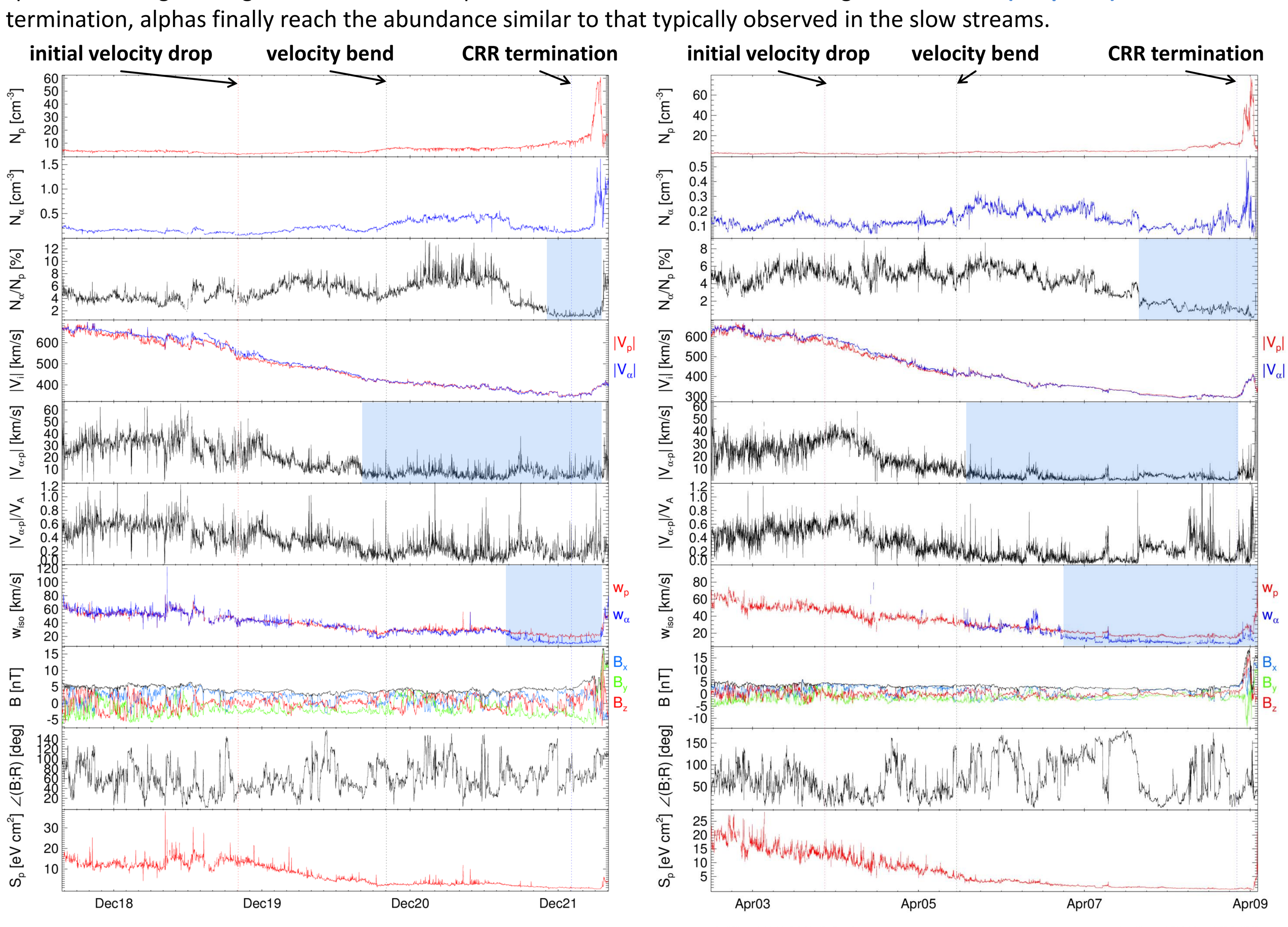

Figure 2: Two examples of the studied CRRs. From top to bottom: proton density, alpha density, relative alpha abundance, proton and alpha bulk speeds, alpha-proton relative drift in units of the local Alfven speed, alpha-proton relative drift in units of the local Alfven speed, proton and alpha thermal speeds, interplanetary magnetic field (IMF) magnitude and its components in the GSE coordinate system, angle between IMF and the radial direction, and specific entropy.

To verify whether these variations are real, we visually inspected the measured ion spectra for the first case and the fitted proton and alpha spectra for different azimuthal angles and various measurement times. Assuming a bi-Maxwellian velocity distribution function (VDF) of incoming ions, SWE Faraday cup (FC) collector current I can be expressed as a function of its collecting area A and the location of the energy window $[V_0, V_0 + \Delta V]$:

$$I = \frac{A q_i n_i}{2}\left[\frac{w_i}{\sqrt{\pi}}\left(e^{-z_0^2} - e^{-z_1^2}\right) + U_z\left(\mathrm{erf}(z_1) - \mathrm{erf}(z_0)\right)\right],$$

where $z_0 = \frac{\sqrt{\frac{2 q_i V_0}{m_i}} - U_z}{w_i}$, $z_1 = \frac{\sqrt{\frac{2 q_i (V_0 + \Delta V_0)}{m_i}} - U_z}{w_i}$, q_i is the ion charge, m_i is the ion mass, n_i is the ion density, w_i is the ion thermal speed and U_z is the ion velocity component in the direction of the Faraday cup normal.

Figure 3 shows that proton and alpha populations were clearly separated in the ion energy spectra for the first case. In the fast stream, the proton beam signature is observed at higher energy-to-charge ratios. However, the data processing did not distinguish the proton beam population. As the proton velocity decreases, the proton beams gradually disappear. After the velocity bend, the alphas develop a strong non-thermal tail, but this feature did not significantly affect the result of fitting. Finally, the solar wind properties begin to match those frequently observed in the slow solar wind streams.

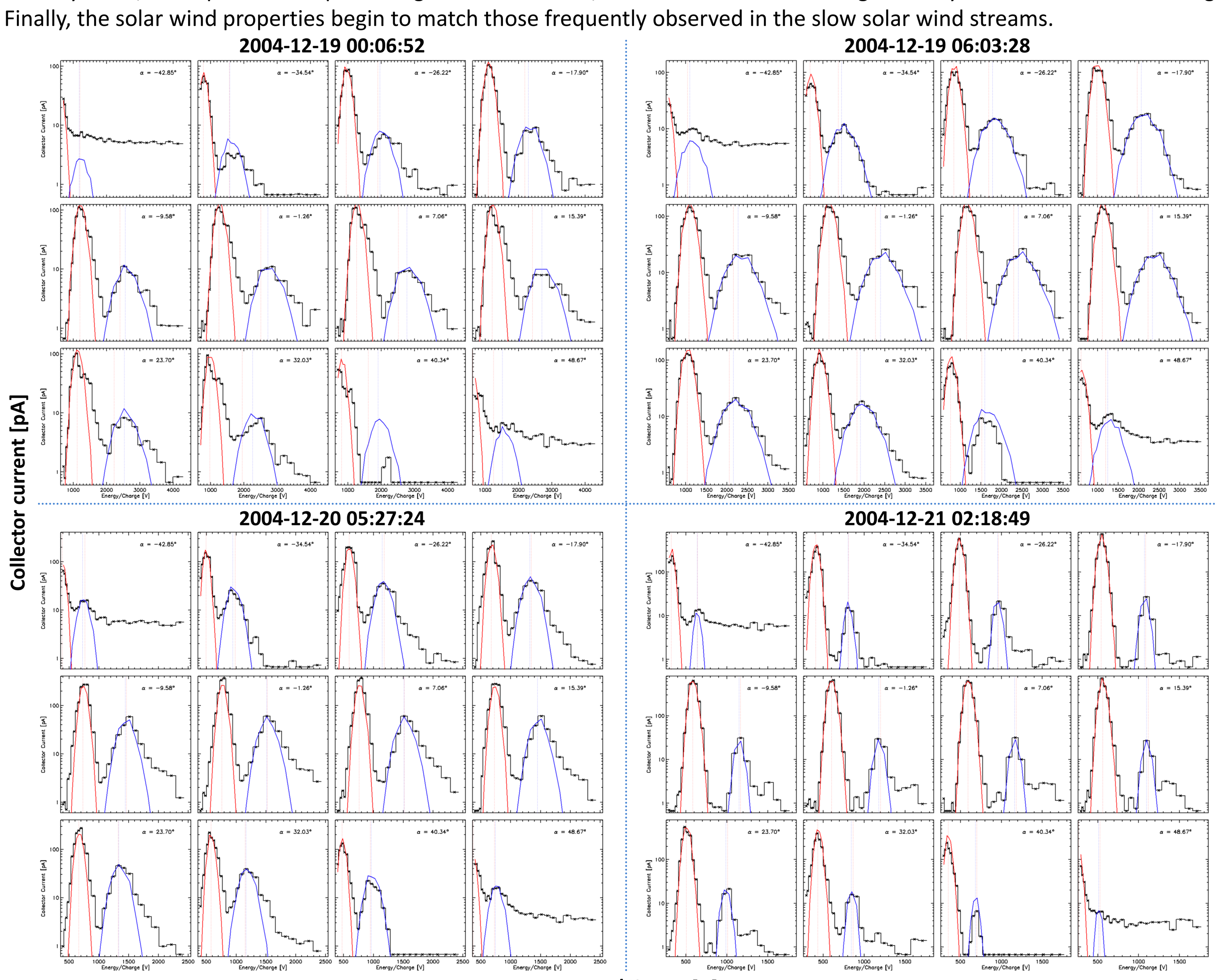

Figure 3: The ion energy spectra for 4 different measurement times. Red and blue curves show the fitted proton and alpha energy spectra. The FC azimuthal angle corresponding to the ion energy spectrum is written in the window upper right corner.

5. Superposed epoch study

How does the global profile of the proton and alpha properties look like across the CRR? In order to answer this question, we performed a superposed epoch analysis of basic ion properties (Figure 4). We found that changes in the alpha properties are temporally separated. Profiles of proton and alpha densities differ after the velocity bend. After the initial velocity drop, the bulk speeds of alphas and protons gradually decrease. Since the deceleration of protons is slower than that of alphas, both components reach almost the same speed already near the velocity bend. The proton and alpha temperatures decrease throughout the CRR. Near the CRR termination, the alpha temperature reaches nearly the same values as the proton temperature and stops decrease.

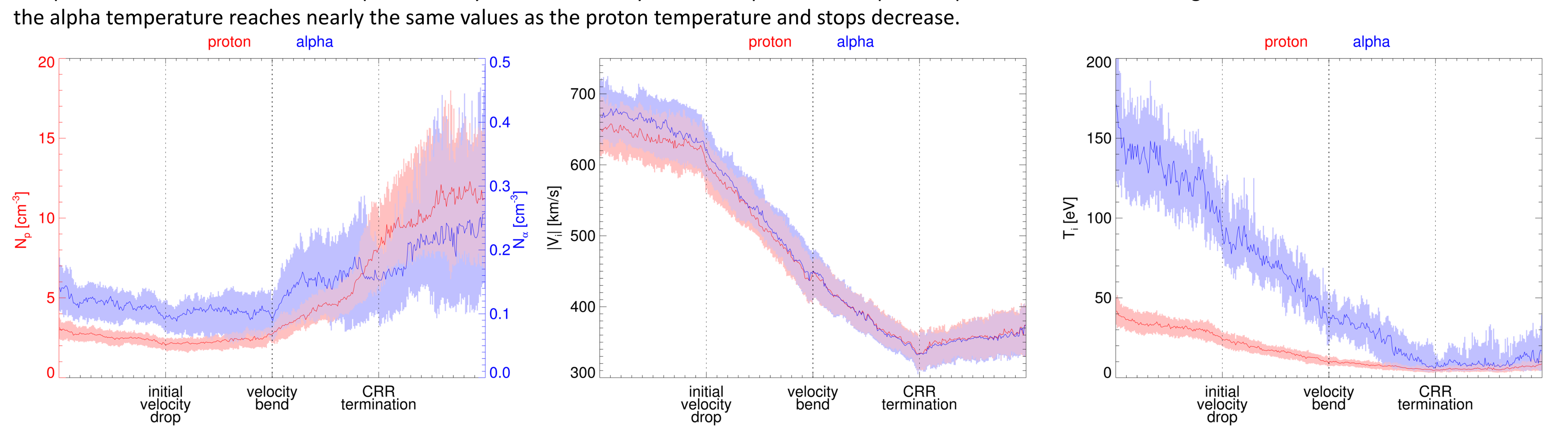

Figure 4: Superposed epoch analysis of the proton (red) and alpha (blue) density (left), bulk speed (center), temperature (right). The solid line shows the median profile and the colored background indicates a region between 25th and 75th percentiles.

We also performed the superposed epoch analysis of the alpha to proton relative properties (Figure 5). The relative alpha abundance increases near the stream interface and then decreases sharply. These abundance changes are not associated with the alpha-proton relative drift variations, as this drift is usually close to zero after the stream interface. The alpha-proton temperature ratio starts to decrease beyond the velocity bend. When the relative alpha abundance reaches values typical for the slow streams, both temperatures are nearly equal.

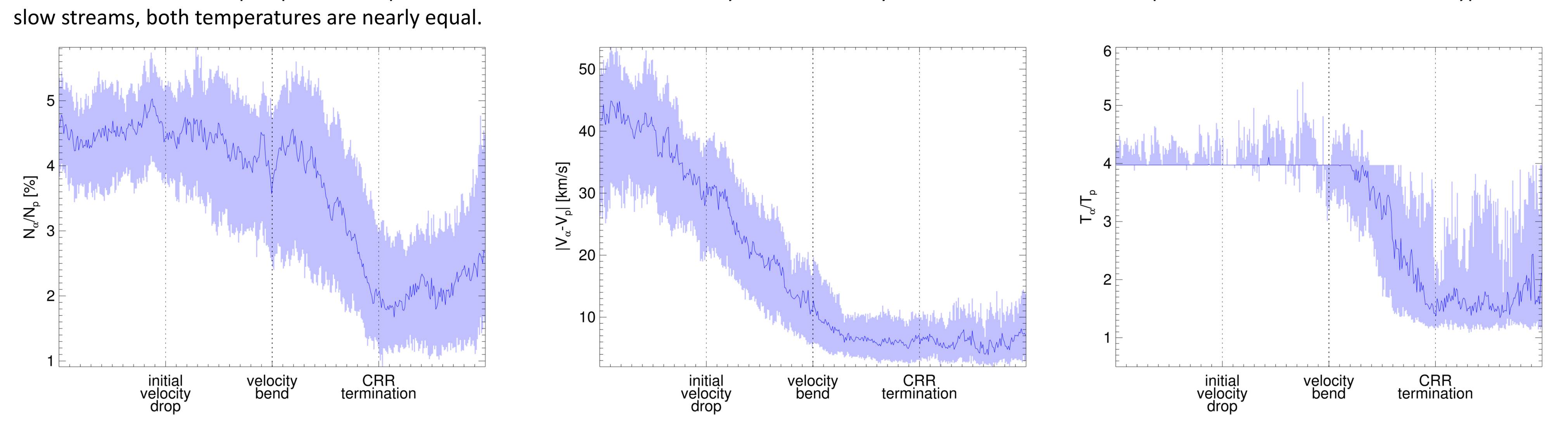

Figure 5: Superposed epoch analysis of the alpha-proton relative abundance (left), magnitude of the alpha-proton relative drift (center) and the alpha-proton temperature ratio (right). The solid line shows the median profile and the colored background indicates a region between 25th and 75th percentiles.

Could these changes in the relative alpha abundance be a signature of a secondary proton population (proton beam)? To answer this question, we prepared superposed epoch analysis of the ratios between the proton parameters calculated as the VDF moment and the corresponding proton parameters obtained from the non-linear fit (Figure 6). The ratio of the proton thermal speeds indicates the presence of a more significant non-thermal part of the proton VDF within CRR. This feature disappears when the relative alpha abundance reaches values typical for the slow solar wind. However, the proton density differs from the density moment by only a few percent. Thus, this cannot fully explain the observed changes in the relative alpha abundance.

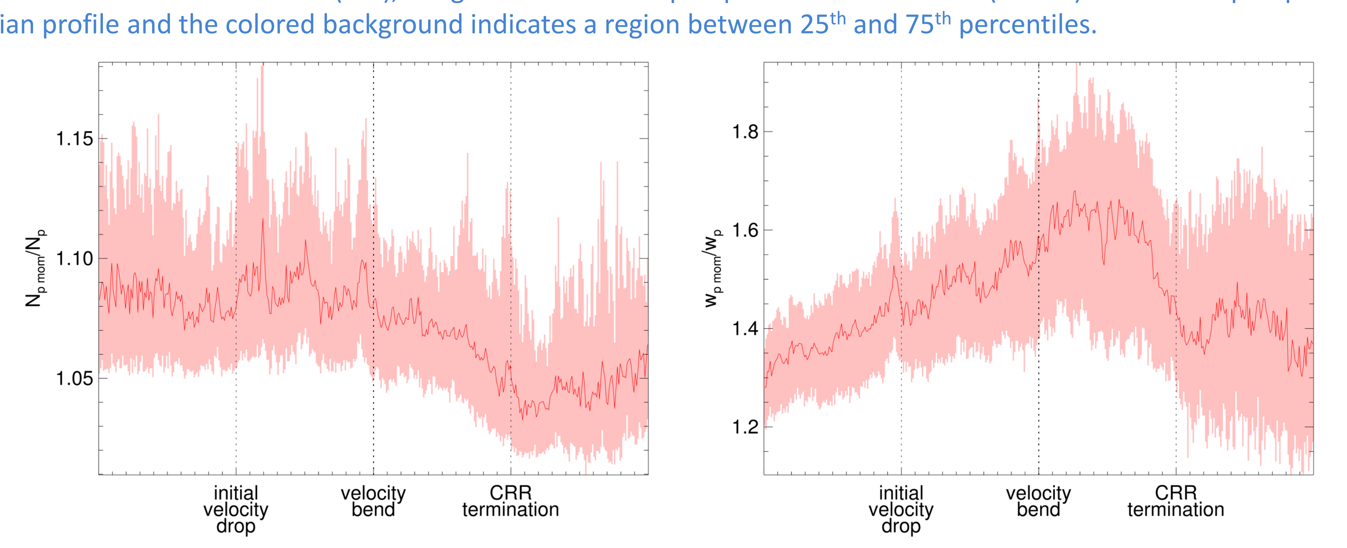

Figure 6: Superposed epoch analysis of the ratio between the proton density (left) and thermal speed (right) estimated from the non-linear fitting and the same parameters computed as the VDF moment.

6. Connection between the alpha properties and other source identifiers

In order to identify possible source regions for the streams observed in the CRRs, we investigated the connection between the alpha properties and other solar wind source identifiers. We started with the differentiation proposed by Fu et al. (2018) (Figure 7). The position of the measurement points in the parameter space proposed by Fu et al. (2018) confirms that the solar wind observed in front of the velocity bend originates from the coronal hole. However, behind the velocity bend, streams from all basic source regions are seemingly observed.

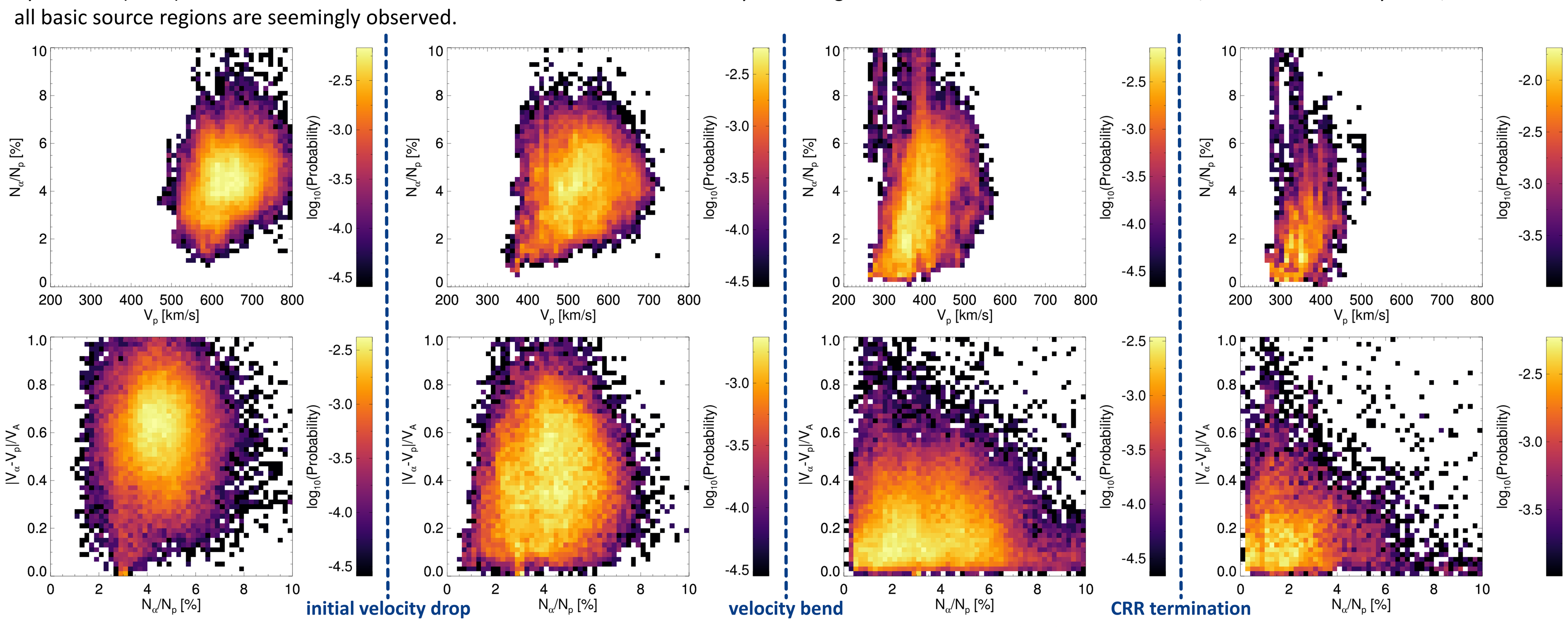

Figure 7: 2D probability distribution of the relative alpha abundance as a function of the proton bulk speed (top), and the alpha-proton relative drift in units of Alfven speed as a function of the relative alpha abundance (bottom) for 4 regions across the CRR marked by dashed blue lines.

Another possible differentiation of the solar wind is by its collisional age (Figure 8, top), A_C which is the ratio of the local expansion time to the local collision timescale. A slightly collisionally older solar wind is observed in front of the velocity bend, but no clear correlation between A_C and $\frac{n_\alpha}{n_p}$ is present. Behind the velocity bend, $\frac{n_\alpha}{n_p}$ decreases with decreasing collisional age. This is associated with the strong correlation between $\frac{n_\alpha}{n_p}$ and the proton thermal speed (Figure 8, bottom).

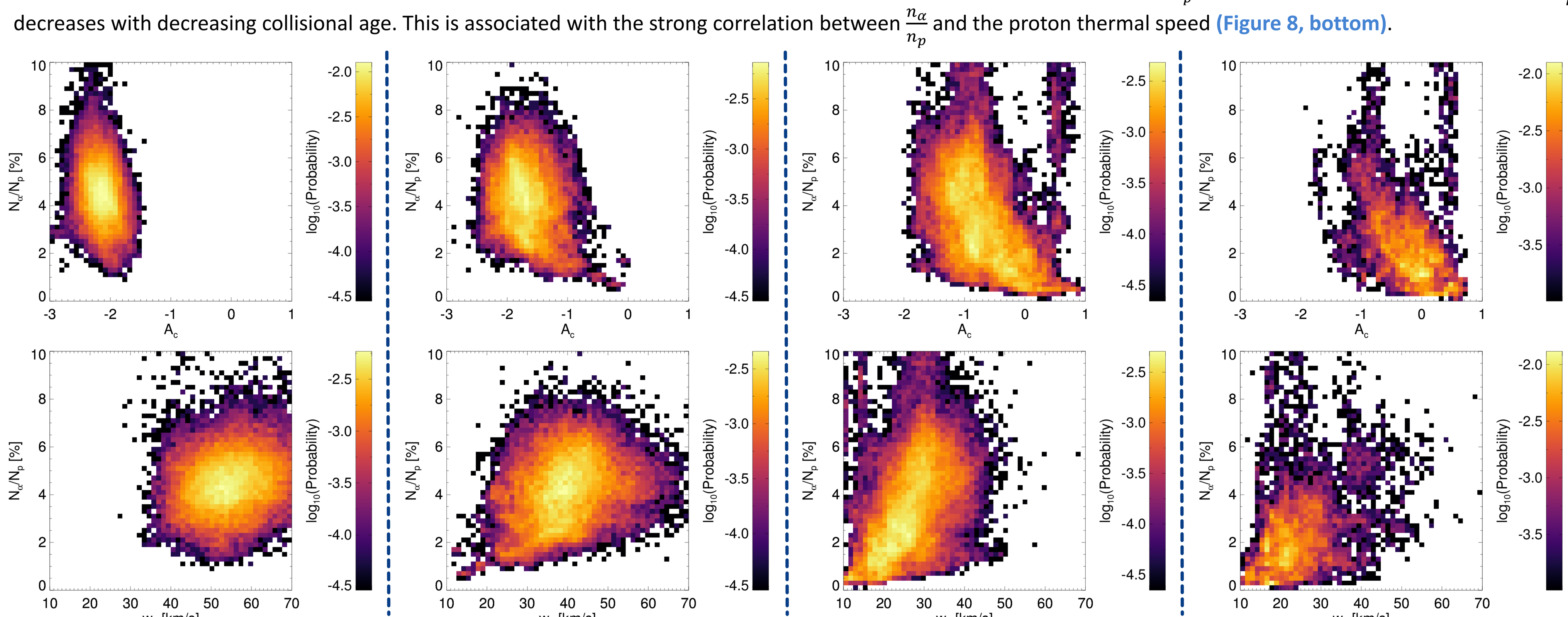

Figure 8: 2D probability distribution of the relative alpha abundance as a function of the collisional age (top) and the proton thermal speed (bottom) for 4 regions across the CRR marked by dashed blue lines.

7. Summary and conclusions

- Using the CRR collection of Borovsky and Denton (2016), we determined global profiles of the alpha parameters across CRR and compared them with those of protons. We consider bi-modal proton VDF composed of the proton core and beam.
- We found that changes in alpha parameters are temporally separated through CRRs:
  - Behind the initial velocity drop, the velocities of alphas and protons gradually decrease. Since the deceleration of protons occurs more slowly than in the case of alphas, both populations reach almost the same speed already near the velocity bend.
  - Around the velocity bend, the increase in the relative alpha abundance is observed. Thereafter, it decreases sharply until the CRR termination is reached.
  - The alpha and proton temperature ratio begins to decrease at the velocity bend. When the relative alpha abundance reaches values typical for the slow streams, both temperatures are nearly equal.
- These changes cannot be fully explained by the proton beam decay alone (see Figs. 3 and 6).
- Comparison between the alpha properties and other solar wind source identifiers suggests that there is a continuous transition from fast to slow solar winds between the velocity bend and the termination of the CRR. This would be consistent with the idea of open field lines moving across the coronal hole boundary as proposed by Schwadron et al. (2002). This may produce streams with mixed alpha properties.

References

- Borovsky, J. E., and Denton, M. H. (2016), The trailing edges of high-speed streams at 1 AU, *J. Geophys. Res. Space Physics*, 121, 6107–6140.
- Ďurovcová, T. et al. (2019), Evolution of the α-proton Differential Motion across Stream Interaction Regions, *The Astrophys. J.,* 873(1), 24.
- Fu, H. et al. (2018), Helium abundance and speed difference between helium ions and protons in the solar wind from coronal holes, active regions, and quiet Sun, *MNRAS*, 478, 1884–1892.
- Schwadron, N. A. (2002), An Explanation for Strongly Underwound Magnetic Field in Co-rotating Rarefaction Regions and its Relationship to Footpoint Motion on the the Sun, *Geophys. Res. Lett.*, 29 (14).

Acknowledgement

This project was supported by the Grant Agency of the Charles University under the project number 264220. We would also like to thank professor Vítek for his continuous support and valuable insight.